EUROFUSION WPS2-PR(16) 15776

W Kernbichler et al.

Solution of drift kinetic equation in stellarators and tokamaks with broken symmetry using the code NEO-2

Preprint of Paper to be submitted for publication in
Plasma Physics and Controlled Fusion

This work has been carried out within the framework of the EUROfusion Consortium and has received funding from the Euratom research and training programme 2014-2018 under grant agreement No 633053. The views and opinions expressed herein do not necessarily reflect those of the European Commission.

Solution of drift kinetic equation in stellarators and tokamaks with broken symmetry using the code NEO-2

W Kernbichler[1], S V Kasilov[1,2], G Kapper[1], A F Martitsch[1], V V Nemov[1,2], C Albert[1], M F Heyn[1]

[1] Institut für Theoretische Physik - Computational Physics, Technische Universität Graz, Fusion@ÖAW, Austria

[2]Institute of Plasma Physics, National Science Center "Kharkov Institute of Physics and Technology", Ukraine

E-mail: winfried.kernbichler@tugraz.at

December 2015

Abstract.

NEO-2 is a linearized drift kinetic equation solver for three-dimensional toroidal magnetic fields. It has been designed in order to treat besides all other regimes effectively the long mean free path regime avoiding any simplifications on device geometry or on the Coulomb collision model. The code is based on the field line integration technique combined with a multiple domain decomposition approach, which allows for introduction of an adaptive grid in velocity space. This makes NEO-2 capable to resolve effectively all boundary layers between various classes of trapped particles and passing particles and also allows for a straightforward code parallelization. In stellarators, NEO-2 is used mainly for computations of neoclassical transport coefficients in regimes with slow plasma rotation and for the evaluation of the generalized Spitzer function, which plays the role of a current drive efficiency. In tokamaks with small ideal non-axisymmetric magnetic field perturbations, NEO-2 is used for evaluation of the toroidal torque resulting from these perturbations (neoclassical toroidal viscosity). The limitation to slow plasma rotation pertinent to usage in stellarators has been removed in this case with help of a quasilinear approach, which is valid due to the smallness of the perturbation field.

1. Introduction

Computations of neoclassical transport coefficients and of the generalized Spitzer function in toroidal plasmas with 3D magnetic fields require the solution of the linearized drift kinetic equation (LDKE) for the perturbation δf of the distribution function $f = f_M + \delta f$ with respect to the local Maxwellian f_M. Since long, this problem is addressed with help of numerical tools [1, 2, 3, 4], which are not limited or have little restrictions on device geometry and provide continuous dependencies of quantities of interest on plasma parameters. This is in contrast to analytical approaches which

are restricted to simplified magnetic field models and to specific confinement regimes. In case of optimized modern stellarator configurations where magnetic fields have high complexity, analytical models can provide only the trends and one has to rely fully upon numerical tools [5]. The dimensionality of the LDKE, which is equal to four in devices without rotational symmetry such as stellarators and tokamaks with 3D magnetic field perturbations, does not present a difficulty for Monte Carlo methods [1, 2, 6, 7, 8]. These methods, however, are relatively CPU intensive and are efficient in computations of phase space integrals such as transport coefficients while computations of the distribution function for those codes constitute a significant difficulty. In contrast, the high problem dimensionality creates a significant difficulty for regular LDKE solvers, which calculate the distribution function using different forms of phase space discretization. Therefore, the problem in these solvers is often simplified by using the mono-energetic approximation based on the Lorentz collision model [3, 4], thus reducing the problem dimension by one. The rest of the collision operator, in particular, the most important momentum conserving part, is then taken into account a posteriori in a truncated version. Numerical models which solve the 4D integro-differential LDKE with the linearized collision operator taken "as is" started to appear only recently [9, 10] with progress in computer power.

It should be noted that all types of LDKE solvers for general regimes (which do not employ a bounce averaging procedure) loose their efficiency in the long mean free path regime where the distribution function becomes a multi-scale function. The variation of its derivative in velocity space boundary layers separating different types of particle orbits (passing and various trapped classes) becomes orders of magnitude higher than in the rest of the velocity space. If problem discretization does not capture these features of the distribution function, the size of the discretized problem grows at best as a square root of the mean free path l_c. In most practical applications this scaling does not prohibit the calculation but, nevertheless, requires rather high computer resources. The NEO-2 LDKE solver [9] described in this paper has been specially designed to overcome this problem using an adaptive velocity space discretization such that the problem size scales logarithmically with l_c. This enables not only a good performance in long mean free path regimes of practical interest but also allows to study the asymptotical limits with l_c exceeding the magnetic field scale by many orders of magnitude. Built originally as a finite collisionality extension of the field line integration technique for the collisionless $1/\nu$ regime [11] where the cross-field particle rotation is negligible, NEO-2 has been used for evaluation of the generalized electron Spitzer function in tokamaks and stellarators [12, 13]. Recently [14], NEO-2 has been generalized including plasma rotation for tokamaks with 3D magnetic fields where the toroidal symmetry is broken by small amplitude perturbations leading to the so called neoclassical toroidal viscosity of the plasma. In this case, the problem is treated in a quasilinear approximation valid for small enough perturbation amplitudes. Details of the analytical treatment and of numerical methods employed in NEO-2 as well as the results of these two rather different applications are the topic of this paper.

The structure of the paper is as follows. In section 2 basic definitions are given introducing the standard neoclassical problem solved by NEO-2. In section 3 the set of problems treated by NEO-2 reducing the problem dimension by one is formulated. The details of the numerical algorithm such as phase space discretization and multiple domain decomposition are discussed in sections 4 and 5. Applications to computation of mono-energetic transport coefficients, of the generalized Spitzer function in stellarators, and of transport coefficients in the perturbed tokamak are presented in section 6. Final remarks are given in section 7.

2. Basic definitions

In flux coordinates $\mathbf{x} = (r, \vartheta, \varphi)$ being the flux surface label (effective radius), poloidal and toroidal angle, respectively, and using the total energy $w = m_\alpha v^2/2 + e_\alpha \Phi$ and the perpendicular adiabatic invariant $J_\perp \approx m_\alpha v_\perp^2 (2\omega_c)^{-1}$ as velocity space variables, with particle charge e_α, particle mass m_α, cyclotron frequency ω_c, velocity module v, and velocity component perpendicular to the magnetic field $v_\perp$, the LDKE is

$$\hat{L}\delta f \equiv v_g^\vartheta \frac{\partial \delta f}{\partial \vartheta} + v_g^\varphi \frac{\partial \delta f}{\partial \varphi} - \hat{L}_C \delta f = -v_g^r \frac{\partial f_M}{\partial r} - e_\alpha E_\parallel v_\parallel \frac{\partial f_M}{\partial w} \equiv -\dot{f}_M. \qquad (1)$$

Here, $\delta f = \delta f(\mathbf{x}, w, J_\perp, \sigma)$, where σ is the parallel velocity sign,

$$v_\parallel = v_\parallel(\mathbf{x}, w, J_\perp, \sigma) = \sigma \sqrt{\frac{2}{m_\alpha}\left(w - e_\alpha \Phi(r) - J_\perp \omega_c(\mathbf{x})\right)}, \qquad (2)$$

$E_\parallel$ is the parallel electric field, $\hat{L}_C$ is the linearized collision operator, $f_M = f_M(r, w)$, and v_g^i are contra-variant components of the guiding center velocity,

$$v_g^i = v_\parallel \frac{\mathbf{B}^* \cdot \nabla x^i}{\mathbf{B}^* \cdot \mathbf{h}}, \qquad \mathbf{B}^* = \mathbf{B} + \nabla \times \left(\frac{v_\parallel}{\omega_c}\mathbf{B}\right), \qquad (3)$$

with $\mathbf{h} = \mathbf{B}/B$ being the unit vector along the magnetic field. Eq. (1) corresponds to the case of mild radial electric fields where the change of kinetic particle energy due to radial drift is small during a single collision time.

Introducing the thermodynamic forces,

$$A_1 = \frac{1}{n_\alpha}\frac{\partial n_\alpha}{\partial r} - \frac{e_\alpha E_r}{T_\alpha} - \frac{3}{2T_\alpha}\frac{\partial T_\alpha}{\partial r}, \quad A_2 = \frac{1}{T_\alpha}\frac{\partial T_\alpha}{\partial r}, \quad A_3 = \frac{e_\alpha \langle E_\parallel B \rangle}{T_\alpha \langle B^2 \rangle}, \qquad (4)$$

where T_α and n_α are α species temperature and density, respectively, $E_r = -\partial\Phi/\partial r$ is the radial electric field and

$$\langle F \rangle = \left(\int_{-\pi}^{\pi} \mathrm{d}\vartheta \int_{-\pi}^{\pi} \mathrm{d}\varphi \sqrt{g} \right)^{-1} \int_{-\pi}^{\pi} \mathrm{d}\vartheta \int_{-\pi}^{\pi} \mathrm{d}\varphi \sqrt{g} F \qquad (5)$$

is the flux surface average of a quantity F with $\sqrt{g}$ being the metric determinant, the full time derivative of the Maxwellian in (1) is presented as follows,

$$\dot{f}_M = -f_M \sum_{k=1}^{3} q_k A_k + \frac{e_\alpha f_M}{T_\alpha} v_\parallel \mathbf{h} \cdot \nabla \delta\Phi. \qquad (6)$$

Here

$$q_1 = -v_g^r, \qquad q_2 = -\frac{m_\alpha v^2}{2T_\alpha} v_g^r, \qquad q_3 = v_\parallel B, \tag{7}$$

and $\delta\Phi$ is the solution of the magnetic differential equation

$$\mathbf{h}\cdot\nabla\delta\Phi = B\frac{\langle E_\parallel B\rangle}{\langle B^2\rangle} - E_\parallel \tag{8}$$

which also satisfies $\langle\delta\Phi\rangle = 0$. The perturbation of the distribution function can be expanded over thermodynamic forces (4) as

$$\delta f = f_M \sum_{k=1}^{3} g_k A_k - \frac{e_\alpha \delta\Phi}{T_\alpha} f_M, \tag{9}$$

where g_k are solutions to

$$\hat{L} f_M g_k = q_k f_M. \tag{10}$$

The last term in (9) follows from the term with $\delta\Phi$ in (6) within the leading order in Larmor radius. Closed within a given species, the representation (9) of δf via the thermodynamic forces is valid if one can ignore the integral part of the linearized collision operator $\hat{L}_C$ for inter-species collisions. This is the case for applications discussed in this paper. In the general case, where kinetic equations (1) for different species are coupled through integral parts of $\hat{L}_C$, the representation of δf for a given species includes thermodynamic forces for all species.

Introducing the thermodynamic fluxes I_k,

$$I_1 = \Gamma_\alpha, \qquad I_2 = \frac{Q_\alpha}{T_\alpha}, \qquad I_3 = n_\alpha \left\langle V_{\parallel\alpha} B\right\rangle, \tag{11}$$

where Γ_α and Q_α, are flux surface averaged particle and energy flux densities, respectively, and $V_{\parallel\alpha}$ is the parallel flow velocity, these fluxes are defined in a general way as

$$I_k = -\left\langle \int \mathrm{d}^3 v\; q_k^\dagger f \right\rangle, \tag{12}$$

where the cross denotes the opposite sign of parallel velocity, $F^\dagger(\mathbf{x}, w, J_\perp, \sigma) = F(\mathbf{x}, w, J_\perp, -\sigma)$, and the velocity space integration is

$$\int \mathrm{d}^3 v\; F = \frac{2\pi e_\alpha}{c\, m_\alpha^3} \sum_{\sigma=\pm} \int_{e_\alpha\Phi}^{\infty} \mathrm{d}w \int_0^{(w-e_\alpha\Phi)/\omega_c} \mathrm{d}J_\perp \frac{B_\parallel^*}{|v_\parallel|}\, F. \tag{13}$$

Fluxes (12) are linked to thermodynamic forces through

$$I_j = -n_\alpha \sum_{k=1}^{3} D_{jk} A_k, \tag{14}$$

where transport coefficients are

$$D_{jk} = \frac{1}{n_\alpha}\left\langle \int \mathrm{d}^3 v\; q_j^\dagger f_M g_k \right\rangle = \frac{1}{n_\alpha}\left\langle \int \mathrm{d}^3 v\; q_j f_M g_k^\dagger \right\rangle, \tag{15}$$

as follows from (9) and the fact that contributions from f_M and from the last term in (9) to the thermodynamic fluxes are zero. Relations (14), which are closed within a single particle species, correspond to the case of a simple plasma being of interest here. In this case, ignoring the slow heat exchange between ions and electrons, the ion problem is decoupled from the electron problem while the latter one is solved for a fixed ion background.

Besides transport coefficients (15), a quantity of particular interest is the generalized Spitzer function

$$g_{\rm sp} = \frac{3\sqrt{\pi}}{4 l_c B_{\rm ref}} g_3, \qquad l_c = \frac{3T_\alpha^2}{4\sqrt{\pi} n_\alpha e_\alpha^4 \Lambda_{\alpha\alpha}}, \tag{16}$$

where $B_{\rm ref}$ is a reference magnetic field (set here to the B_{00} harmonic of the magnetic field strength in Boozer coordinates), l_c is the mean free path and $\Lambda_{\alpha\alpha}$ is the Coulomb logarithm.

It should be noted that solutions of the linearized kinetic equation are determined up to the function of two arbitrary constants, $C_n + C_v v^2$, which re-defines density and temperature in the Maxwellian. These constants are removed by additional constraints

$$\left\langle \int \mathrm{d}^3 v \; f_M g_k \right\rangle = \left\langle \int \mathrm{d}^3 v \; v^2 f_M g_k \right\rangle = 0. \tag{17}$$

3. Phase space variables and reduction of the spatial dimension by one

The truncated guiding center velocity in the linear operator $\hat{L}$ in (1) preserves kinetic energy. Therefore, a convenient choice for velocity space variables is the velocity module v and the normalized perpendicular adiabatic invariant $\eta = v_\perp^2/(v^2 B) = (1-\lambda^2)/B$, which are invariants of this truncated motion. In contrast to the pitch parameter $\lambda = v_\parallel/v$, the normalized invariant η is more suited for adaptive discretization of the velocity space in the long mean free path regime where a rapid variation of the distribution function in this space is localized within boundary layers $\eta \approx \eta_i = const$ between velocity space regions occupied by passing particles and by various classes of trapped particles.

3.1. Slow cross-field rotation

NEO-2 treats two particular cases where the spatial dimension of the problem can be reduced by one. The first case corresponds to transport regimes in general toroidal magnetic field geometry where the cross-field drift has a negligible effect on decorrelation of particles and magnetic field. In these regimes cross-field rotation can be ignored in angular components of the guiding center velocity. In field aligned coordinates $(r, \vartheta, \varphi_0)$ where $\varphi_0 = \varphi - q\vartheta$ labels field lines and $q = 1/\iota$ is the safety factor, the evolution operator $\hat{L}$ truncated to leading order in Larmor radius takes the form

$$\hat{L} \to \hat{L}_0 = v\lambda h^\vartheta \frac{\partial}{\partial \vartheta} - \hat{L}_C = v\lambda \frac{\partial}{\partial l} - \hat{L}_C, \tag{18}$$

where l is the distance counted along the field line and $\lambda = \sigma\,(1-\eta B)^{1/2}$. In this case, equations (10) describe the distribution function on a single infinite field line which densely covers the magnetic flux surface. Respectively, various flux surfaces averages (5) are represented by field line averages as follows

$$\langle F\rangle = \lim_{\vartheta_{\max}\to\infty}\left(\int\limits_{\vartheta_{\min}}^{\vartheta_{\max}}\frac{\mathrm{d}\vartheta}{B^{\vartheta}}\right)^{-1}\int\limits_{\vartheta_{\min}}^{\vartheta_{\max}}\frac{\mathrm{d}\vartheta}{B^{\vartheta}}F = \lim_{L\to\infty}\left(\int\limits_{0}^{L}\frac{\mathrm{d}l}{B}\right)^{-1}\int\limits_{0}^{L}\frac{\mathrm{d}l}{B}F. \qquad (19)$$

In practice, a finite field line is used which is long enough to represent the whole magnetic flux surface. This field line starts at the poloidal cut $\varphi = \varphi_{\mathrm{cut}}$ and, after passing a large number of toroidal field periods, ends on the same cut. The number of these periods is chosen in such a way that the last field line footprint on the cut, $\vartheta = \vartheta_{\max}$, is close enough to the first footprint $\vartheta = \vartheta_{\min}$ so that the field line can be treated as a closed field line, $\vartheta_{\max} \approx \vartheta_{\min} + 2\pi N_{\max}$ where $N_{\max}$ is an integer value.

It should be noted that evaluation of transport coefficients in this formulation generally does not require a magnetic field representation in flux coordinates and can be performed also for magnetic fields given in real space coordinates. All necessary data on the magnetic field geometry entering Eqs. (10) are obtained in the latter case with help of a preliminary integration of the magnetic field line equations together with an additional set of linear ODEs which determine the normal ∇r to the flux surface (see Refs. [15, 11]). The latter quantity is required in the sources (7) where it determines the radial guiding center velocity via the geodesic curvature of the field line k_G as follows,

$$v_g^r = \frac{v^2(2-\eta B)}{2\omega_c}k_G|\nabla r|. \qquad (20)$$

Respectively, k_G is defined in flux and real space coordinates by

$$k_G|\nabla r| = \frac{1}{\sqrt{g}B^2}\left(\left(B_\vartheta + qB_\varphi\right)\frac{\partial B}{\partial\varphi_0} - B_\varphi\frac{\partial B}{\partial\vartheta}\right) = \frac{1}{B}\left(\mathbf{h}\times\nabla B\right)\cdot\nabla r, \qquad (21)$$

where B_ϑ and B_φ are the co-variant magnetic field components in periodic flux coordinates.

The leading order evolution operator (18) with reversed velocity sign, $\hat{L}_0^\dagger$, is adjoint to $\hat{L}_0$. Namely, for any F and G the following identity is fulfilled,

$$\left\langle\int \mathrm{d}^3v\; G\hat{L}_0 f_M F\right\rangle = \left\langle\int \mathrm{d}^3v\; F\hat{L}_0^\dagger f_M G\right\rangle. \qquad (22)$$

Onsager symmetry of transport coefficients (15) is a particular consequence of this property,

$$\begin{aligned} n_\alpha D_{jk} &= \left\langle\int \mathrm{d}^3v\; q_j^\dagger f_M g_k\right\rangle = \left\langle\int \mathrm{d}^3v\; g_k\hat{L}_0^\dagger f_M g_j^\dagger\right\rangle \\ &= \left\langle\int \mathrm{d}^3v\; q_k f_M g_j^\dagger\right\rangle = n_\alpha D_{kj}. \end{aligned} \qquad (23)$$

In a similar way, current driven by the resonant interaction of waves with plasma described by the quasilinear diffusion operator $\hat{L}_{QL}$,

$$\hat{L}\,\delta f_{RF} = Q_{RF} \equiv \hat{L}_{QL} f_M, \qquad (24)$$

is reduced to a convolution of the RF phase space source density Q_{RF} with the adjoint generalized Spitzer function (16),

$$\begin{aligned}\left\langle j_{\alpha\parallel}B\right\rangle &= -e_\alpha\left\langle\int \mathrm{d}^3v\; q_3^\dagger\delta f_{RF}\right\rangle = -e_\alpha\left\langle\int \mathrm{d}^3v\; g_3^\dagger\hat{L}_0\delta f_{RF}\right\rangle \\ &= -e_\alpha l_c B_{\mathrm{ref}}\left\langle\int \mathrm{d}^3v\; g_{\mathrm{sp}}^\dagger Q_{RF}\right\rangle. \end{aligned} \tag{25}$$

3.2. Perturbed tokamak equilibria

The second case where the spatial dimension of the problem can be reduced retaining now plasma rotation is the case of an axially symmetric (tokamak) magnetic field with small non-axisymmetric perturbations. If the perturbation amplitude is small enough such that the effect of the perturbation field on particle motion within the flux surface is negligible, a reduction of the dimension is achieved with help of a quasilinear approximation expanding the distribution function in field aligned coordinates $(r, \vartheta, \varphi_0)$ in a series over the perturbation field (see Ref. [14]). In field aligned coordinates constructed from periodic Boozer coordinates, the only important magnetic field characteristic which is not axially symmetric (depends on the field line label φ_0) is the magnetic field magnitude B. Expanding B and solutions to (10) in Fourier series over φ_0,

$$\begin{aligned} B(\vartheta,\varphi_0) &= \mathrm{Re}\sum_{n=0}^{\infty} B_n(\vartheta)\mathrm{e}^{in\varphi_0}, \\ g_k(\vartheta,\varphi_0,v,\eta,\sigma) &= \mathrm{Re}\sum_{n=0}^{\infty} g_{kn}(\vartheta,v,\eta,\sigma)\mathrm{e}^{in\varphi_0}, \end{aligned} \tag{26}$$

each of equations (10) is split into an equation for the axisymmetric parts of the distribution functions g_{k0},

$$\hat{L}_0 g_{k0} f_M = q_k f_M, \tag{27}$$

and equations for complex Fourier amplitudes g_{kn} of the non-axisymmetric part of this function, $n > 0$,

$$\hat{L}_0 g_{kn} f_M + in\Omega_t g_{kn} f_M = q_{kn} f_M - v\lambda h^\vartheta \eta f_M \left(\frac{\partial}{\partial\vartheta}\frac{B_n}{B_0}\right)\frac{\partial g_{k0}}{\partial\eta} - \frac{B_n}{B_0}\hat{L}_C g_{k0} f_M, \tag{28}$$

which describe g_{kn} in leading (linear) order over the perturbation field amplitude B_n/B_0. Quantities h^ϑ, λ, ω_c and $\sqrt{g}$, which appear in Eq. (28) and enter Eq. (27) via the definition (18) of the operator $\hat{L}_0$ and definitions (7), (20), (21) of source amplitudes q_k, correspond here to the unperturbed, axisymmetric field $B_0 = B_0(r,\vartheta)$, and also the normalized invariant η is defined through the unperturbed field B_0. The source amplitudes q_{kn} in (28) are defined in the same way as q_k except for a different definition of the geodesic curvature,

$$k_G|\nabla r| \to \frac{1}{\sqrt{g}}\left(\frac{inB_n}{B_0 h^\vartheta} - B_\varphi\frac{\partial}{\partial\vartheta}\frac{B_n}{B_0^2}\right), \tag{29}$$

and the toroidal rotation frequency Ω_t due to $\mathbf{E}\times\mathbf{B}$ and magnetic drift corresponds in (28) to the axisymmetric magnetic field,

$$\Omega_t = \frac{cE_r}{\sqrt{g}B_0 h^\vartheta} + \frac{v^2\left(2-\eta B_0\right)}{2\sqrt{g}B_0\omega_c}\left(\frac{B_r}{B_0}\frac{\partial B_0}{\partial\vartheta} - \frac{1}{h^\vartheta}\frac{\partial B_0}{\partial r}\right) + \frac{v^2\left(1-\eta B_0\right)}{\sqrt{g}B_0\omega_c}\left(\frac{\partial B_\vartheta}{\partial r} + q\frac{\partial B_\varphi}{\partial r} - \frac{\partial B_r}{\partial\vartheta}\right). \tag{30}$$

Due to periodicity of the functions g_{kn},

$$g_{kn}(\vartheta+2\pi,v,\eta,\sigma) = g_{kn}(\vartheta,v,\eta,\sigma)\mathrm{e}^{2\pi i n q}, \tag{31}$$

equations (27) and (28) are solved within a single poloidal field period $0<\vartheta<2\pi$. In the quasilinear approximation, transport coefficients (15) are presented as a sum of axisymmetric and non-axisymmetric contributions, $D_{jk} = D_{jk}^{\mathrm{AX}} + D_{jk}^{\mathrm{NA}}$, where axisymmetric (ambipolar) transport coefficients D_{jk}^{AX} are directly given by (15) with $g_k = g_{k0}$ and the axisymmetric q_k introduced in Eq. (27). Flux surface average (5) and velocity space integration (13) in (15) corresponds here to the axisymmetric field, where integration over φ is trivial. In Boozer coordinates where on a given flux surface $\sqrt{g}$, $1/B^\vartheta$, and $1/B^2$ are linked through constant factors, one can present

$$\left\langle\int \mathrm{d}^3v F\right\rangle = \pi\left(\int_0^{2\pi}\frac{\mathrm{d}\vartheta}{B_0^2}\right)^{-1}\int_0^{2\pi}\frac{\mathrm{d}\vartheta}{B_0}\sum_{\sigma=\pm}\int_0^\infty \mathrm{d}v v^2\int_0^{1/B_0}\mathrm{d}\eta\frac{F}{\sqrt{1-\eta B_0}}. \tag{32}$$

The same expression follows also from (19) due to periodicity of subintegrands. Non-axisymmetric contributions to transport coefficients D_{1k} which determine the non-ambipolar particle flux density responsible for the NTV torque consist of independent contributions from separate toroidal harmonics,

$$D_{1k}^{\mathrm{NA}} = -\sum_{n=1}^\infty \frac{n}{4n_\alpha\omega_c\sqrt{g}h^\vartheta}\left\langle\int \mathrm{d}^3v v^2 f_M\frac{2-\eta B_0}{B_0}\mathrm{Im}\; g_{kn}B_n^*\right\rangle, \tag{33}$$

where the average is given by (32), $k=1$ or 2, and the Ware pinch coefficient D_{13}^{NA} is negligible.

4. Discretization

The three dimensional kinetic equations of the previous section, in particular, Eqs. (27) and (28) can be generally cast in the following form,

$$v\lambda h^\vartheta f_M\frac{\partial g}{\partial\vartheta} + i\omega f_M g - \hat{L}_C f_M g = q f_M. \tag{34}$$

The energy dependence of the solutions is discretized with help of the Galerkin method. Presenting

$$g(\vartheta,v,\eta,\sigma) = \sum_{m'=0}^M g_{m'}(\vartheta,\eta,\sigma)\varphi_{m'}(v), \tag{35}$$

where $\varphi_{m'}(v)$ is some set of basis functions, multiplying Eq. (34) with $v^3\varphi_m(v)$ and integrating over v, the kinetic equation is reduced to a coupled set of 2D equations for the expansion coefficients $g_m(\vartheta,\eta)$,

$$\lambda h^\vartheta \frac{\partial g_m}{\partial \vartheta} + \sum_{m'=0}^{M} \left(i\omega_{mm'} - \hat{L}_{C,mm'} \right) g_{m'} = q_m, \tag{36}$$

where the matrices

$$\begin{aligned} \omega_{mm'} &= \int_0^\infty \mathrm{d}v v^3 \varphi_m(v) \omega(\vartheta,v,\eta) f_M(v) \varphi_{m'}(v), \\ \hat{L}_{C,mm'} &= \int_0^\infty \mathrm{d}v v^3 \varphi_m(v) \hat{L}_C f_M(v) \varphi_{m'}(v), \\ q_m &= \int_0^\infty \mathrm{d}v v^3 \varphi_m(v) q(\vartheta,v,\eta,\sigma) f_M(v), \end{aligned} \tag{37}$$

are independent of v. Expressions (37) are valid for orthogonal basis functions such that the matrix

$$\rho_{mm'} = \int_0^\infty \mathrm{d}v v^4 f_M(v) \varphi_m(v) \varphi_{m'}(v) \tag{38}$$

is a unit matrix, $\rho_{mm'} = \delta_{mm'}$. Up to a normalization coefficient C_m, these basis functions are identical to generalized Laguerre polynomials of the order 3/2, $\varphi_m(v) = C_m L_m^{3/2}(z)$, where $z = m_\alpha v^2/(2m_\alpha T_\alpha)$ is the normalized kinetic energy. In a more general case of a non-orthogonal basis, matrices entering Eqs. (35) are obtained from matrices (37) by multiplying them with $\rho^{-1}_{mm'}$ which is the inverse of (38),

$$\omega_{mm'} = \sum_{m''=0}^{M} \rho^{-1}_{mm''} \omega^{(37)}_{m''m'}, \qquad \text{etc.} \tag{39}$$

Matrix elements of the collision operator, $\hat{L}_{C,mm'}$, are integro-differential operators with respect to the variable η,

$$\begin{aligned} \hat{L}_{C,mm'} g_m = \kappa &\left(2\nu_{mm'} \lambda \frac{\partial}{\partial \eta} \frac{\lambda \eta}{B} \frac{\partial}{\partial \eta} + D_{mm'} \right) g_m(\vartheta,\eta,\sigma) \\ &+ \kappa \sum_{l=0}^{L} I^l_{mm'} P_l(\lambda) \int_{-1}^{1} \mathrm{d}\lambda' P_l(\lambda') g_m(\vartheta,\eta',\sigma'), \end{aligned} \tag{40}$$

where $P_l(\lambda)$ are Legendre polynomials, $\eta' = \eta(\vartheta,\lambda')$ and $\sigma' = \mathrm{sign}(\lambda')$. Constant coefficients $\nu_{mm'}$, $D_{mm'}$ and $I^l_{mm'}$ which correspond to scattering over pitch-angle and energy by field particles and to the scattering by test particles (integral part of linearized collision operator), respectively, are determined by the basis φ_m and are independent of plasma parameters which enter Eq. (40) only via the inverse mean free path length $\kappa = 1/l_c$, where l_c is defined in (16). As already mentioned above, the integral part of

the collision operator is taken into account here only for like particle collisions. The only coefficients where collisions with other species are taken into account are $\nu_{mm'}$ for electrons where ions are included in the infinite ion mass limit.

An important particular case often used in neoclassical transport modelling is the mono-energetic model where the Lorentz collision operator covering only pitch-angle scattering is employed. In this case, the equation set (36) is reduced to a single equation, $m = m' = 0$, with the source term q_0 being a respective source (7) divided by v, $D_{00} = I^l_{00} = 0$, $\nu_{00} = 1$, and $l_c = v/\nu_D$ where $\nu_D = \nu_D(v)$ is the deflection frequency.

For the numerical solution, the set of 2D equations (36) is discretized on a non-equidistant (ϑ, η) grid using the conservative finite difference (finite volume) scheme, which is of third order over η and of first or second order over ϑ. This grid is adaptive over η in order to resolve the boundary layers where the gradient of the distribution function scales with $l_c^{1/2}$ and may increase there by few orders of magnitude in long mean free path regimes. Due to this grid property, scaling of the η-grid size with l_c is logarithmic.

The resulting set of linear algebraic equations is solved taking into account the integral part of the collision operator by iterations. In this way functions g_m in the subintegrand of (40) are known from the previous iteration, and the equation set for g_m on the next iteration is sparse enough in order to be efficiently solved by sparse solvers based on L-U decomposition. Such a straightforward method is used in NEO-2 for the quasilinear problem discussed in section 3.2 where due to periodicity the problem is limited to a single poloidal field period and only one boundary layer exists. In case of a general 3D stellarator geometry discussed in section 3.1 the ϑ-domain may cover several hundred periods. In addition, since $B(\vartheta)$ is aperiodic within the domain, various classes of trapped particles appear whose number scales with the field line length. Therefore, the use of a global adaptive grid is practically impossible because its dimension scales in the long mean free path regime as square of the field line length and this is definitely incompatible with available computer memory. A method suitable for this case is discussed in the next section.

5. Multiple domain decomposition

In the case of a general 3D geometry the field line is split into multiple domains where the kinetic equation is solved independently in terms of propagators. The discretization grid is individual for each domain where it is adapted only to relevant boundary layers. For simplicity this method is formulated here for the mono-energetic model where equation (10) with explicit substitution of (18) and the truncated version of the collision operator (40), i.e., the Lorentz collision operator, is

$$\sigma \frac{\partial g_k^\sigma}{\partial \vartheta} - \frac{\partial}{\partial \eta} \frac{2\kappa|\lambda|\eta}{B^\vartheta} \frac{\partial g_k^\sigma}{\partial \eta} = s_k^\sigma. \tag{41}$$

Here and below, a compact new notation is used for the distribution functions $g_k^\sigma = g_k^\sigma(\vartheta, \eta) = g_k(\vartheta, \varphi_0, v, \eta, \sigma)$ and the source terms $s_k^\sigma = s_k^\sigma(\vartheta, \eta) =$

$q_k(\vartheta, \varphi_0, v, \eta, \sigma)(|\lambda|h^\vartheta)^{-1}$. Expressions for mono-energetic transport coefficients are obtained replacing in (15) $f_M(v) \to n_\alpha \delta(v - v_0)/(4\pi v^2)$ and using (19) with finite field line closure $\vartheta_{\max}$,

$$D_{jk}^{\text{mono}} = \frac{1}{4}\left(\int_{\vartheta_{\min}}^{\vartheta_{\max}} \frac{\mathrm{d}\vartheta}{B^\vartheta}\right)^{-1} \gamma_{jk}(\{\text{tot}\}),$$

$$\gamma_{jk}(\{\text{tot}\}) = \int_{\vartheta_{\min}}^{\vartheta_{\max}} \mathrm{d}\vartheta \sum_{\sigma=\pm} \int_0^{1/B} \mathrm{d}\eta s_j^{-\sigma} g_k^\sigma. \tag{42}$$

The notation $\{\text{tot}\}$ is used here to indicate the fact that $\gamma_{jk}(\{\text{tot}\})$ has to be computed for the whole (total) field line.

5.1. Propagator method

The local solution to (41) within a given domain N along the field line where $\vartheta_N^- < \vartheta < \vartheta_N^+$ is fully determined if boundary conditions are set for incoming particles, i.e. $g_k^+(\vartheta_N^-, \eta)$ and $g_k^-(\vartheta_N^+, \eta)$, are specified,

$$g_k^\sigma(\vartheta, \eta) = \sum_{\sigma'=\pm} \int_0^{1/B(\vartheta_N^{-\sigma'})} \mathrm{d}\ \eta' G_{\sigma'}^\sigma(\vartheta, \eta, \eta') g_k^{\sigma'}(\vartheta_N^{-\sigma'}, \eta') + g_{k(\text{loc})}^\sigma(\vartheta, \eta). \tag{43}$$

Here $g_{k(\text{loc})}^\sigma(\vartheta, \eta)$ is the solution to (41) with homogeneous boundary conditions $g_{k(\text{loc})}^\sigma(\vartheta_N^{-\sigma}, \eta) = 0$, and Greens function $G_{\sigma'}^\sigma(\vartheta, \eta, \eta')$ is the solution to the homogeneous form of Eq. (41). It satisfies the boundary conditions $G_{\sigma'}^\sigma(\vartheta_N^{-\sigma}, \eta, \eta') = \delta_{\sigma\sigma'}\delta(\eta - \eta')$, where $\delta_{\sigma\sigma'}$ is similar to the Kronecker symbol, $\delta_{++} = \delta_{--} = 1$ and $\delta_{+-} = \delta_{-+} = 0$. Eq. (43) demonstrates the fact that for the computation of $g_k^\sigma(\vartheta, \eta)$ at a given position ϑ within a domain, contributions which propagate from the left boundary ($\sigma' = +$) and from the right boundary ($\sigma' = -$) have to be added to the local contribution $g_{k(\text{loc})}^\sigma(\vartheta, \eta)$.

To characterize now a given domain N, one introduces propagators and integral local sources, respectively, as follows

$$A_{\sigma'}^\sigma(\{N\}, \eta, \eta') \equiv G_{\sigma'}^\sigma(\vartheta_N^\sigma, \eta, \eta'), \tag{44}$$

$$Q_k^\sigma(\{N\}, \eta) \equiv g_{k(\text{loc})}^\sigma(\vartheta_N^\sigma, \eta). \tag{45}$$

Using $\vartheta_N^\pm = \vartheta_{N\pm1}^\mp$, the outgoing distributions to the neighboring domains $N \pm 1$ are expressed with help of (43) through outgoing distributions from these domains, which are the same as the incoming ones for domain N, $g_k^\pm(\vartheta_N^\mp, \eta) = g_k^\pm(\vartheta_{N\mp1}^\pm, \eta)$, as follows,

$$g_k^\sigma(\vartheta_N^\sigma, \eta) = \sum_\pm \hat{A}_\pm^\sigma(\{N\}) g_k^\pm(\vartheta_{N\mp1}^\pm, \eta) + Q_k^\sigma(\{N\}, \eta), \tag{46}$$

where the integral operators $\hat{A}_\pm^\sigma(\{N\})$ are defined via

$$\hat{A}_{\sigma'}^\sigma(\{N\})F(\eta) = \int_0^{1/B(\vartheta_N^{-\sigma'})} \mathrm{d}\eta' A_{\sigma'}^\sigma(\{N\}, \eta, \eta') F(\eta'). \tag{47}$$

The contribution of the domain N to field line integrals γ_{jk} is expressed trough the outgoing distributions from neighboring domains as

$$\gamma_{jk}(\{N\}) = \sum_{\pm} \mathring{Q}_{j\pm}(\{N\}) g_k^{\pm}(\vartheta_{N\mp1}^{\pm}, \eta) + \gamma_{jk}^{(\mathrm{loc})}(\{N\}), \tag{48}$$

where

$$\mathring{Q}_{j\sigma}(\{N\}) F(\eta) = \int_0^{1/B(\vartheta_N^{-\sigma})} \mathrm{d}\eta \; Q_{j\sigma}(\{N\}, \eta) F(\eta) \tag{49}$$

is an integral functional, and where

$$Q_{j\sigma}(\{N\}, \eta) \equiv \int_{\vartheta_N^-}^{\vartheta_N^+} \mathrm{d}\vartheta \sum_{\sigma'=\pm} \int_0^{1/B(\vartheta)} \mathrm{d}\eta' \; s_j^{-\sigma'}(\vartheta, \eta') G_{\sigma}^{\sigma'}(\vartheta, \eta', \eta), \tag{50}$$

$$\gamma_{jk}^{(\mathrm{loc})}(\{N\}) \equiv \int_{\vartheta_N^-}^{\vartheta_N^+} \mathrm{d}\vartheta \sum_{\sigma=\pm} \int_0^{1/B(\vartheta)} \mathrm{d}\eta \; s_j^{-\sigma}(\vartheta, \eta) g_{k(\mathrm{loc})}^{\sigma}(\vartheta, \eta). \tag{51}$$

The set of 2D functions (44), 1D functions (45) and (50), and constants (51) is denoted as $\mathbf{\Pi}(\{N\})$,

$$\mathbf{\Pi}(\{N\}) = \left\{ A_{\sigma'}^{\sigma}(\{N\}, \eta, \eta'),\; Q_k^{\sigma}(\{N\}, \eta),\; Q_{j\sigma}(\{N\}, \eta),\; \gamma_{jk}^{(\mathrm{loc})}(\{N\}) \right\}. \tag{52}$$

This set fully characterizes the local domain, and it is convenient to use the name "propagator" for such sets rather than for functions (44).

For the total solution of the problem, the procedure which combines propagators of adjacent domains resulting in a propagator for the joint domain, $\mathbf{\Pi}(\{N\}) \circ \mathbf{\Pi}(\{N+1\}) = \mathbf{\Pi}(\{N\} + \{N+1\}) \equiv \mathbf{\Pi}(\{+\})$, is defined using Eqs. (46) and (48) in these two domains and eliminating the distribution function at the common boundary $\vartheta_N^+ = \vartheta_{N+1}^-$,

$$\begin{aligned}
\hat{A}_+^+(\{+\}) &= \hat{A}_+^+(\{N+1\})\, \hat{B}_+^+\, \hat{A}_+^+(\{N\}), \\
\hat{A}_-^+(\{+\}) &= \hat{A}_+^+(\{N+1\})\, \hat{B}_-^+\, \hat{A}_-^-(\{N+1\}) + A_-^+(\{N+1\}), \\
\hat{A}_+^-(\{+\}) &= \hat{A}_-^-(\{N\})\, \hat{B}_+^-\, \hat{A}_+^+(\{N\}) + A_+^-(\{N\}), \\
\hat{A}_-^-(\{+\}) &= \hat{A}_-^-(\{N\})\, \hat{B}_-^-\, \hat{A}_-^-(\{N+1\}), \\
Q_k^+(\{+\}) &= \hat{A}_+^+(\{N+1\}) \left(\hat{B}_+^+\, Q_k^+(\{N\}) + \hat{B}_-^+\, Q_k^-(\{N+1\}) \right) \\
&\quad + Q_k^+(\{N+1\}), \\
Q_k^-(\{+\}) &= \hat{A}_-^-(\{N\}) \left(\hat{B}_+^-\, Q_k^+(\{N\}) + \hat{B}_-^-\, Q_k^-(\{N+1\}) \right) \\
&\quad + Q_k^-(\{N\}), \\
\mathring{Q}_{j+}(\{+\}) &= \left(\mathring{Q}_{j+}(\{N+1\})\, \hat{B}_+^+ + \mathring{Q}_{j-}(\{N\})\, \hat{B}_+^- \right) A_+^+(\{N\}) \\
&\quad + \mathring{Q}_{j+}(\{N\}), \\
\mathring{Q}_{j-}(\{+\}) &= \left(\mathring{Q}_{j+}(\{N+1\})\, \hat{B}_-^+ + \mathring{Q}_{j-}(\{N\})\, \hat{B}_-^- \right) A_-^-(\{N+1\})
\end{aligned} \tag{53}$$

$$
\begin{aligned}
&+ \mathring{Q}_{j-}(\{N+1\}),\\
\gamma_{jk}^{(\mathrm{loc})}(\{+\}) &= \mathring{Q}_{j+}(\{N+1\})\left(\hat{B}_+^+\, Q_k^+(\{N\}) + \hat{B}_-^+\, Q_k^-(\{N+1\})\right)\\
&+ \mathring{Q}_{j-}(\{N\})\left(\hat{B}_+^-\, Q_k^+(\{N\}) + \hat{B}_-^-\, Q_k^-(\{N+1\})\right)\\
&+ \gamma_{jk}^{(\mathrm{loc})}(\{N\}) + \gamma_{jk}^{(\mathrm{loc})}(\{N+1\}),
\end{aligned}
$$

where the argument η has been dropped in $Q_k^\sigma(\{N\}) \equiv Q_k^\sigma(\{N\},\eta)$. Integral operators $\hat{B}_{\sigma'}^\sigma$ in (53) are defined as follows,

$$
\hat{B}_{\sigma'}^\sigma F(\eta) = \int_0^{1/B(\vartheta_N^+)} \mathrm{d}\eta' B_{\sigma'}^\sigma(\eta,\eta') F(\eta'), \tag{54}
$$

where the kernels are the solutions to the following set of integral equations,

$$
\begin{aligned}
B_{\sigma'}^+(\eta,\eta') - \hat{A}_-^+(\{N\}) B_{\sigma'}^-(\eta,\eta') &= \delta_{\sigma'+}\delta(\eta-\eta'),\\
-\hat{A}_+^-(\{N+1\}) B_{\sigma'}^+(\eta,\eta') + B_{\sigma'}^-(\eta,\eta') &= \delta_{\sigma'-}\delta(\eta-\eta').
\end{aligned} \tag{55}
$$

Finally, combining all propagators,

$$
\mathbf{\Pi}(\{1\}) \circ \mathbf{\Pi}(\{2\}) \circ \ldots \circ \mathbf{\Pi}(\{N_{\max}\}) = \mathbf{\Pi}\left(\sum_{N=1}^{N_{\max}} \{N\}\right) \equiv \mathbf{\Pi}\left(\{\mathrm{tot}\}\right), \tag{56}
$$

and imposing periodicity conditions at the field line ends, $g_k^\sigma(\vartheta_{N_{\max}}^+,\eta) = g_k^\sigma(\vartheta_1^-,\eta)$, where $\vartheta_1^- = \vartheta_{\min}$ and $\vartheta_{N_{\max}}^+ = \vartheta_{\max}$, generalized relations (46) turn into a set of integral equations for the distribution functions at the ends,

$$
g_k^\sigma(\vartheta_1^-,\eta) = \sum_\pm \hat{A}_\pm^\sigma(\{\mathrm{tot}\}) g_k^\pm(\vartheta_1^-,\eta) + Q_k^\sigma(\{\mathrm{tot}\},\eta). \tag{57}
$$

Transport coefficients (42) are expressed through the solution of this equation with help of (48) as follows,

$$
\gamma_{jk}(\{\mathrm{tot}\}) = \sum_\pm \mathring{Q}_{j\pm}(\{\mathrm{tot}\}) g_k^\pm(\vartheta_1^-,\eta) + \gamma_{jk}^{(\mathrm{loc})}(\{\mathrm{tot}\}). \tag{58}
$$

Computation of the distribution functions (in particular the Spitzer function) requires the knowledge of these functions at domain boundaries (see the formal solution (43)). Solutions at all these boundaries are obtained from known solutions at the periodic boundary by backward recursion where the unknown $g_k^\sigma(\vartheta_N^-,\eta)$ are obtained from the known $g_k^\sigma(\vartheta_{N+1}^-,\eta)$ by solving the set of integral equations

$$
\begin{aligned}
g_k^+(\vartheta_N^-,\eta) - \hat{A}_-^+(\{\mathrm{C}\}) g_k^-(\vartheta_N^-,\eta) &= \hat{A}_+^+(\{\mathrm{C}\}) g_k^+(\vartheta_1^-,\eta) + Q_k^+(\{\mathrm{C}\},\eta),\\
-\hat{A}_+^-(\{N\}) g_k^+(\vartheta_N^-,\eta) + g_k^-(\vartheta_N^-,\eta) &= \hat{A}_-^-(\{N\}) g_k^-(\vartheta_{N+1}^-,\eta) + Q_k^-(\{N\},\eta),
\end{aligned} \tag{59}
$$

where cumulative propagators

$$
\mathbf{\Pi}(\{\mathrm{C}\}) \equiv \mathbf{\Pi}\left(\sum_{N'=1}^{N} \{N'\}\right) \tag{60}
$$

are already available as by-products of the computation of $\mathbf{\Pi}(\{\mathrm{tot}\})$.

In the discretized problem, all integral operations on propagator quantities are replaced by matrix multiplications. Therefore, integral equations are reduced to sets of linear algebraic equations. Although the matrices are not sparse, their size is rather moderate, because it is determined by the size of the η-grid, which is rather limited due to the adaptive nature of this grid. Due to the adaptive η-grid which differs from domain to domain (see next subsection), in the discretized problem a third order rediscretization scheme is employed to match the solutions at domain boundaries when joining propagators.

The case of the full linearized collision operator is similar to the mono-energetic example shown here. The main difference is that distribution functions g_k^σ in (43) become vectors with respect to the test function index m and Green functions $G_{\sigma'}^\sigma$ turn into matrices, what introduces some complexity in the notation and is therefore omitted here.

5.2. Adaptive grid

The local discretization grids in (ϑ, η)-variables for the finite volume method are adapted in NEO-2 to the plasma collisionality using a binary refinement method. Such a refinement is required in the long mean free path regime where $L_c/l_c \ll 1$ with $L_c = 2\pi R_0$ and R_0 being the reference major radius of the torus. In such regimes with mild radial electric field values, the scale of the solution over the normalized perpendicular invariant η changes from the $\delta\eta B \sim 1$ in most regions of the phase space to $\delta\eta B \sim \sqrt{L_c/l_c} \ll 1$ in layers formed around boundaries $\eta = \eta_i \equiv 1/B_i^{\max}$, where $B_i^{\max} \equiv B(\vartheta_i)$ are local magnetic field maxima on a given field line, $i = 1, 2, \ldots$.

These boundaries separate various particle classes with collisionless orbits containing different numbers of local magnetic field minima between their pertinent reflection points (trapped particles) and the class of passing particles is separated from trapped ones by the global field maximum. In contrast to the axisymmetric field where all local maxima have the same (global) value and, therefore, only one boundary layer and one class of trapped particles exist, the number of local maxima (and, respectively, of trapped particle classes) grows linearly with the field line length. This makes the generation of a global η-grid with a feasible size practically impossible. However, not all of these maxima produce local boundary layers at a given point ϑ, but only those, "relevant" $B_i^{\max}$ which can be accessed along the orbit by a particle with $\eta = 1/B_i^{\max}$ starting at ϑ, i.e., those $B_i^{\max}$ which form two increasing sequences when moving in both directions from the adjacent field maxima ordered according to $|\vartheta - \vartheta_i|$. The number of these relevant maxima scales logarithmically with the field line length allowing to resolve all relevant boundary layers locally within a finite ϑ domain. Since relevant maxima are the same for all points ϑ in the domain between two neighboring local maxima, $\vartheta_i < \vartheta < \vartheta_{i+1}$, such domains called "ripples" below, are used for the problem decomposition discussed in section 5 (some of the ripples can be split further at period boundaries).

The η-scale of the solution in a particular boundary layer induced by a relevant local maximum i can be represented by the η-scale of the Gaussian,

$$G_i(\vartheta,\eta) = \frac{1}{\sqrt{2\pi}\Delta\eta_i}\exp\left(-\frac{(\eta-\eta_i)^2}{2\Delta\eta_i^2}\right), \tag{61}$$

where $\Delta\eta_i = \Delta\eta_i(\vartheta) = \max(\Delta\eta, \Delta\eta_{\min})$, and

$$\Delta\eta = \left|4\kappa\eta_i \int\limits_{\vartheta_i}^{\vartheta} \mathrm{d}\vartheta' \frac{\lambda(\vartheta',\eta_i)}{B^\vartheta(\vartheta')}\right|^{1/2}, \qquad \Delta\eta_{\min} \sim \frac{\kappa}{B^\vartheta(\vartheta_i)}\left|\eta_i \frac{\partial^2 B(\vartheta_i)}{\partial\vartheta_i^2}\right|^{-1/2}. \tag{62}$$

The quantity $\Delta\eta$ in (62) corresponds to the asymptotical fundamental solution of the homogeneous version of Eq. (41) with the initial condition at $\vartheta = \vartheta_i$ and $\Delta\eta_{\min}$ represents the solution scale in the vicinity of this maximum point. The adaptive η-grid is formed locally in a given ripple starting from the global (usually equidistant) base grid and using binary refinement, which minimizes the absolute error of fixed order Lagrange polynomial interpolation of the test function (61) at some fixed ϑ within the domain. The refinement may be subsequently repeated for a different ϑ, and this procedure is performed for all relevant local maxima. In the numerical realization, within each ripple the following local values are used, $\Delta\eta_i(\vartheta_i)$, $\Delta\eta_{i+1}(\vartheta_{i+1})$, and $\Delta\eta_{i'}(\vartheta_{\min,i})$, where $\vartheta_i < \vartheta_{\min,i} < \vartheta_{i+1}$ is the position of the field minimum within the given ripple, and indices i' correspond to all relevant maxima. Quantities $\Delta\eta_{i'}(\vartheta_{\min,i})$ are taken into account by an approximate solution of the integral in (62) between the position of relevant maximum $\vartheta_{i'}$ and $\vartheta_{\min,i}$.

This kind of refinement is sufficient for the mono-energetic problem. In the general case, the mono-energetic refinement is repeated for a few energies from the thermal energy up to several thermal energies. The refinement does not need very accurate evaluation of integrals (62). Therefore, this can be performed with low CPU cost. Since the number of nodes of the refined grid scales as $|\log\Delta\eta_i|$ and the scaling of the number of relevant maxima with field line length is also logarithmic, the η-grid has a feasible size for rather low plasma collisionalities. The ϑ-grid is refined afterwards by adding to the equidistant base ϑ-grid the intersection points of η_i levels with the phase space boundary $\eta B(\vartheta) = 1$. For low collisionalities, the dense η-grid around $1/B_i^{\max}$ ensures also a rather dense ϑ-grid close to the pertinent field maximum. Thus, a proper resolution of distribution functions is ensured.

Examples of the grid for different collisionalities are shown in Figs. 1 and 2.

6. Applications

6.1. Mono-energetic transport coefficients in a stellarator

In Fig. 3 two normalized mono-energetic transport coefficients, namely, the diffusion coefficient, D_{11}^*, and the bootstrap coefficient, D_{31}^*, are shown for the W-7X standard configuration as functions of the collisionality parameter $\nu^* = R_0/(\iota l_c)$ where R_0 is the major radius and l_c is the mono-energetic mean free path defined in section 4.

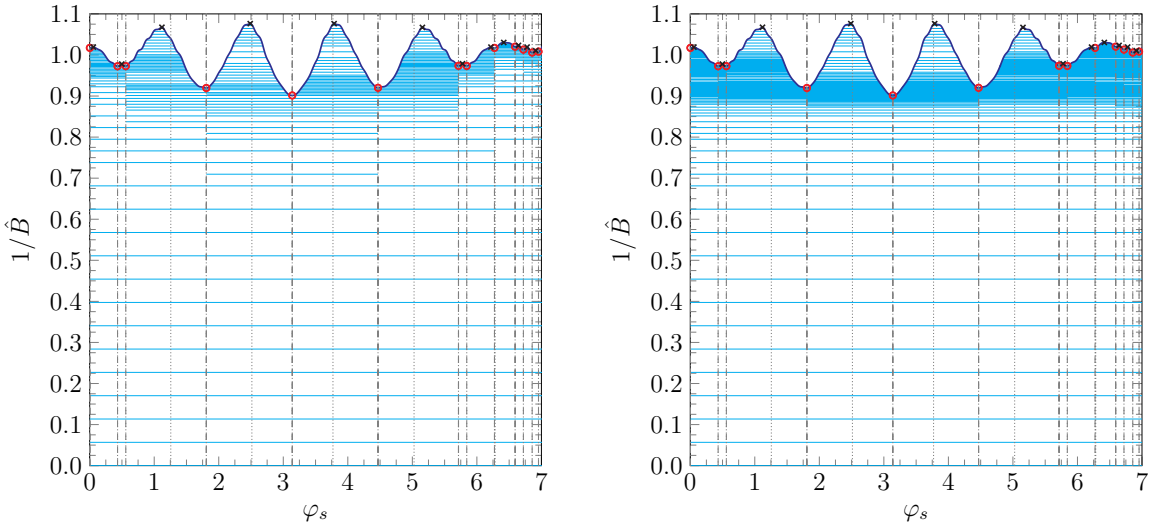

Figure 1. η-levels (horizontal lines) at $L_c/l_c = 2 \cdot 10^{-1}$ (left) and $L_c/l_c = 2 \cdot 10^{-4}$ (right) and $1/\hat{B}$ (blue solid line) along the field line. Ripple boundaries are depicted as vertical dashed lines, toroidal field period boundaries are depicted as vertical dotted lines. Local minima and maxima of $\hat{B} = B/B_{\mathrm{ref}}$ are indicated as black crosses and red circles, respectively.

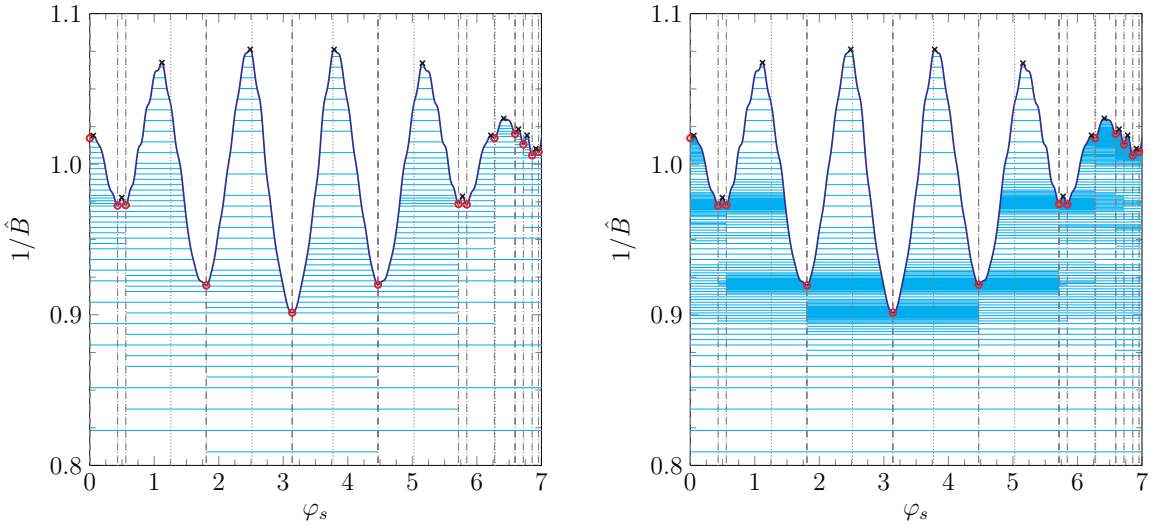

Figure 2. Zoomed depiction of Figure 1 with $L_c/l_c = 2{\cdot}10^{-1}$ (left) and $L_c/l_c = 2{\cdot}10^{-4}$ (right).

Normalization of coefficients as well as the definition of ν^* are the same as in Ref. [5], $D_{11}^* = D_{11}/D_{11}^p$ and $D_{31}^* = D_{31}/D_{31}^b$ where D_{11}^p and D_{31}^b are transport coefficients in the equivalent tokamak in plateau and banana regimes, respectively. For the comparison, asymptotical values of transport coefficients computed by the code NEO in the $1/\nu$-regime are shown where D_{11} and D_{31} are computed according to Ref. [11] and Refs. [16, 17], respectively. In contrast to D_{11}^* which quickly reaches the asymptotical value when reducing collisionality, the bootstrap coefficient D_{31}^* remains different from

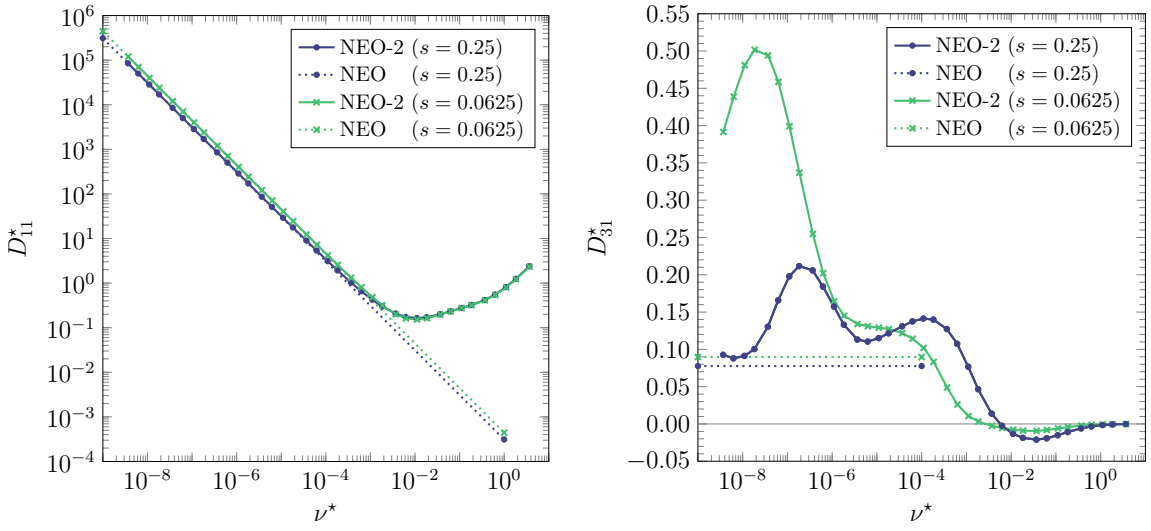

Figure 3. Normalized mono-energetic radial transport coefficient $D_{11}^\star$ (left) and normalized mono-energetic bootstrap current coefficient $D_{31}^\star$ (right) as a function of collisionality computed by NEO-2 (solid) for finite collisionalities and by NEO (dotted) for the collisionless limit at half radius $s = 0.25$ (circles) and quarter radius $s = 0.0625$ (crosses). Markers on the solid lines correspond to results of NEO-2 runs at given collisionalities.

the asymptotic value even if ν^* is smaller than one by many orders of magnitude. This trend has been shown earlier in Ref. [5] for a few different configurations up to $\nu^* \sim 10^{-6}$, and is seen here up to $\nu^* = 3 \cdot 10^{-9}$. It has been also shown there that even a small $\mathbf{E} \times \mathbf{B}$ rotation allows to reach the asymptotical value of D_{31}^* (see Fig. 26 of Ref. [5] for respective W-7X dependencies).

Such a behavior of D_{31} is not a computational artefact which could be expected at extremely low collisionalities: It is well reproduced for different field line settings (starting point and number of periods) and different base grid parameters (resulting finally in different refined η-grids). The result well fulfills the Onsager symmetry ($D_{31} = D_{13}$) which is not an intrinsic property of the NEO-2 discretization scheme but is used instead as a convergence measure.

Deviations of D_{31} from the ideal $1/\nu$ limit are caused by a collisional effect of trapped particles on the passing particle distribution. This effect is fully ignored in analytical theory for infinitesimal collisionalities when setting for the passing particle distribution function g_1 (driven by the source q_1, see Eq. (7)) the boundary condition at the trapped-passing boundary where g_1 is assumed to be equal to the collisionless radial displacement of the orbit starting at the flux surface from the global maximum point (see also [18]). At this point the parallel velocity is zero for transient particles and, respectively, co- and counter-passing distribution functions are equal. In this ideal picture the trapped particle region is excluded from the formation of the bootstrap current and contributes only to the Pfirsch-Schlüter current. The distribution of the latter current over velocity space represented by g_1^a being the odd part of g_1 is rather

peculiar in stellarators. A significant part of this current flows in the trapped region within boundary layers $\eta \approx \eta_i$ separating different trapped particle classes. In these layers g_1^a scales as $\nu^{-1/2}$ in case of finite collisionality and turns into a δ-function in the infinitesimal collisionality limit, $g_1^a \sim \delta(\eta - \eta_i)$. If this limit is enforced, all η_i layers are clearly separated from the passing particle region and do not influence the passing particle distribution. However, for any small but finite collisionality, always classes exist at irrational flux surfaces with a boundary layer widths comparable to the distance from η_i to the trapped-passing boundary. Contributions from such boundary layers effectively modify the passing particle distribution at the trapped-passing boundary and thus modify the value of the bootstrap current. In more details this effect will be discussed in a separate publication.

6.2. Spitzer function in stellarators

The application of NEO-2 to computations of the generalized Spitzer function $g_{\rm sp}$, Eq. (16), in a stellarator with finite plasma collisionality is illustrated in Figs. 5 and 6 where $g_{\rm sp}$ is shown for the standard W7-X configuration at half of the plasma radius, $s = 0.25$, with locations specified in Fig. 4.

The plasma collisionality $L_c/l_c = 2 \cdot 10^{-2}$ in this example corresponds to the long mean free path regime, $\nu_d R_0/(v_T \iota \varepsilon_M^{3/2}) = L_c/(2\pi l_c \iota \varepsilon_M^{3/2}) \approx 0.1 \ll 1$ where $\iota = 0.87$ and $\varepsilon_M \approx 0.09$ are the rotational transform and the field modulation amplitude, respectively, and $v_T = (2T_e/m_e)^{1/2}$ is the thermal velocity.

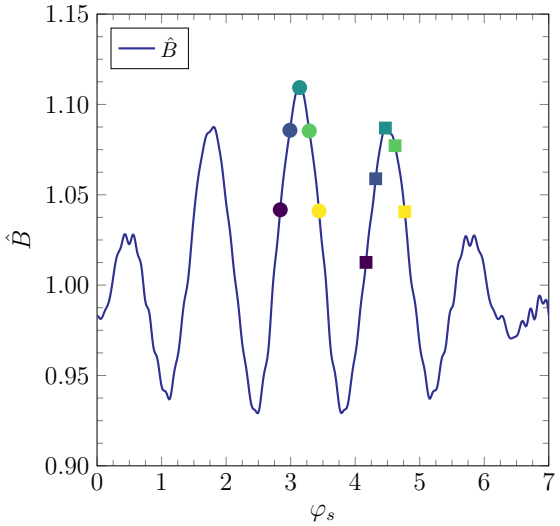

Figure 4. Normalized magnetic field module $\hat{B} = B/B_{\rm ref}$ vs. the field line parameter $\varphi_s = \iota\vartheta$ and points for plotting $g_{\rm sp}$ near the global maximum (colored circles) and local maximum (colored squares).

The Spitzer function is plotted for a few spatial points at the field line passing through the global maximum (see Fig. 4) with locations around this maximum (Fig. 5) and around the nearest local maximum (Fig. 6). The results of NEO-2 are compared

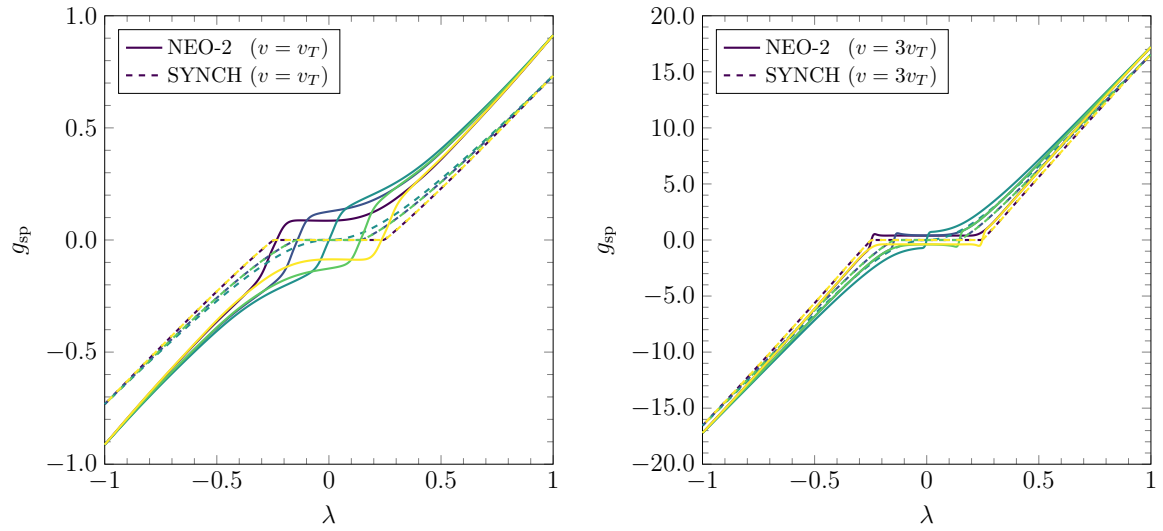

Figure 5. Generalized Spitzer function vs. pitch angle parameter λ for $v = v_T$ (left) and $v = 3v_T$ (right) computed for finite collisionality (solid) and in the collisionless limit (dashed) at points around global maximum marked in Fig. 4 with filled circles. Lines colors correspond to respective marker colors.

with the collisionless limit computed by the code SYNCH [19] shown in Figs. 5 and 6 with dashed lines. In contrast to the collisionless limit as well as to the high collisionality limit

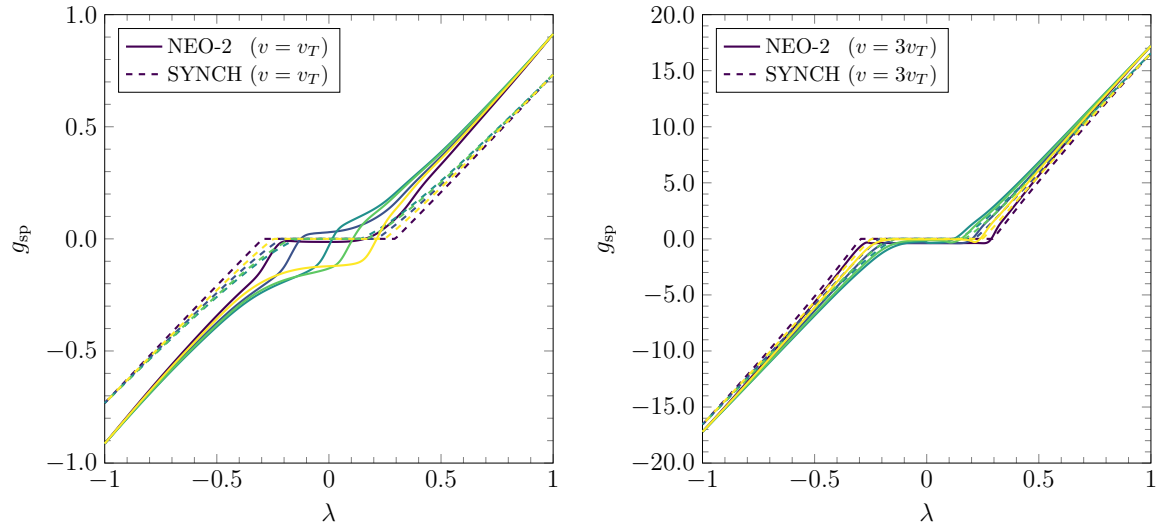

Figure 6. The same as in Fig. 5 for points around local maximum marked in Fig. 4 with filled squares.

where the Spitzer function is an odd function of λ, this function has no distinct parity in case of finite plasma collisionality (see also Refs. [12, 13]). The even part of g_{sp} pertinent to the finite collisionality case permits current drive by phase space sources symmetric with respect to λ, see Eq. (25). It can be produced, in particular, by the resonant absorption of waves with symmetric parallel wave number spectra [20]. The magnitude

and the direction of a current driven by such sources is mainly determined by the spatial location of the source (location of the wave absorption region). The mechanism responsible for this type of current drive is actually the same as the mechanism of bootstrap current generation, where the symmetric phase space sources $q_{1,2}f_M A_{1,2}$ are produced by the radial particle drift in presence of radial plasma parameter gradients (compare (25) with the definition (15) of bootstrap coefficients D_{31} and D_{32}).

6.3. Neoclassical Toroidal Viscosity

An application of the quasilinear transport model of section 3.2 to a tokamak with small amplitude magnetic perturbations is demonstrated in Fig. 7 where the non-axisymmetric ion transport coefficient D_{11}^{NA} computed by NEO-2 is compared to asymptotical models. Non-ambipolar radial particle fluxes determined by D_{11}^{NA} and D_{12}^{NA} are responsible in tokamaks for the neoclassical toroidal viscous torque which is directly related to these fluxes via the flux-force relation [16, 21, 14]. This example corresponds to a tokamak with circular concentric flux surfaces and perturbation in the form of a single toroidal harmonic, $B(\vartheta,\varphi) = B_0(\vartheta)(1+\varepsilon_M \cos(n\varphi))$ where $\varepsilon_M = 10^{-3}$. The diffusion coefficient is shown in the normalized form, $\hat{D}_{11}^{*} = D_{11}^{\mathrm{NA}} D_p^{-1}$ where $D_p = \pi q v_T \rho_L^2/(16R)$ is the plateau diffusion coefficient and $\rho_L = v_T/\omega_c$ is the Larmor radius for the reference magnetic field, as function of the plasma collisionality parameter $\nu_f^* = 2qR_0 l_c^{-1}$ for a few distinct values of the radial electric field specified via the toroidal Mach number $M_t = R_0\Omega_{tE}/v_T$ where Ω_{tE} is the toroidal $\mathbf{E}\times\mathbf{B}$ rotation frequency determined by the first term in Eq. (30). Results correspond to a flux surface with aspect ratio $A = 10$ and toroidal harmonic number $n = 3$. The toroidal rotation due to the magnetic drift has been set to zero in (30) for all Mach numbers except $M_t = 10^{-5}$ while for $M_t = 10^{-5}$ this drift has been included for the ion temperature $T_i = 6.5 e_i \psi_{\mathrm{tor}} |\Omega_{tE}|/c$, where ψ_{tor} is the toroidal flux. Asymptotical models used for the comparison are indicated in the caption. It can be seen that NEO-2 accurately reproduces all asymptotical regimes in their validity domains. In particular, collisionless plateau diffusion, which corresponds at low collisionalities to the resonant diffusion regime at $M_t \geq 2.8\cdot 10^{-2}$ and to the superbanana-plateau regime at $M_t = 10^{-5}$, is well resolved. The perturbed distribution in these regimes is highly localized around resonant curves in velocity space what presents a significant numerical difficulty in case of non-adaptive velocity space discretization.

7. Conclusion

Among the existing numerical tools for computation of neoclassical transport coefficients and of the generalized Spitzer function in 3D toroidal geometries, NEO-2 is a specific one with an improved performance in the long mean free path regime. Such a performance is achieved with help of an adaptive phase space discretization and multiple domain decomposition. These techniques result in a logarithmic scaling of required computer resources (memory and CPU time) with plasma collisionality. In addition, the linearized

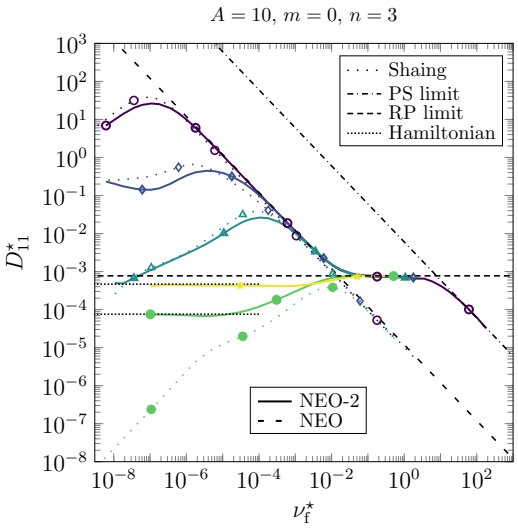

Figure 7. Normalized diffusion coefficient $\hat{D}_{11}^{\mathrm{NA}}$ from NEO-2 (solid line) and bounce-averaged model of Shaing [21] (loosely dotted line) as functions of collisionality ν^* for various toroidal Mach numbers $M_t = 2.8{\cdot}10^{-7}$ ($\circ$), 10^{-5} ($\Diamond$), $2.8{\cdot}10^{-4}$ ($\triangle$), $2.8{\cdot}10^{-2}$ ($\bullet$) and $6{\cdot}10^{-2}$ ($\star$). The collisionless limits for the $1/\nu$ regime (loosely dashed line) and the resonant diffusion regime (densely dotted line) are computed by NEO [11] and a semi-analytical model based on a Hamiltonian approach [22], respectively. The diffusion coefficients for the ripple-plateau regime [23] and the Pfirsch-Schlüter regime [24, 25] are shown with a densely dashed line and a dash-dotted line, respectively.

collision operator has been realized in NEO-2 without model simplifications. These two properties of the code allow to use it as benchmarking tool for different analytical and numerical models especially at low collisionalities where computations with NEO-2 remain feasible even for $\nu^* \sim 10^{-8}$. The code employs the field line integration technique, which also permits computations in magnetic fields specified in real space (cylindrical) coordinates. Direct practical applications of the code to general 3D toroidal geometries are presently limited to the case of weak radial electric fields such that cross field particle rotation can be ignored. This is the case if finite plasma collisionality effects on the generalized electron Spitzer function is of interest. Those effects are absent at high and low collisionality limits. The above limitation on cross field rotation is absent in case of tokamaks with small amplitude non-axisymmetric magnetic field perturbations, which are treated by NEO-2 in a quasilinear approximation. Such an approximation covers most of the transport regimes of interest for the computation of the neoclassical toroidal viscosity where it permits fast and accurate evaluation of transport coefficients. NEO-2 is currently an evolving tool, and the limitations mentioned above are not of principal nature. Therefore, further extensions of NEO-2 should permit more general applications without a loss of good code performance.

Acknowledgments

This work has been carried out within the framework of the EUROfusion Consortium and has received funding from the Euratom research and training programme 2014-2018 under grant agreement No 633053. The views and opinions expressed herein do not necessarily reflect those of the European Commission. The computational results presented have been achieved in part using the Vienna Scientific Cluster (VSC).

References

[1] A. H. Boozer and G. Kuo-Petravic. Monte Carlo evaluation of transport coefficients. *Phys. Fluids*, 24(5):851–859, 1981.

[2] W. Lotz and J. Nührenberg. Monte Carlo computations of neoclassical transport. *Phys. Fluids*, 31(10):2984–2991, 1988.

[3] S. P. Hirshman, K. C. Shaing, W. I. van Rij, C. O. Beasley, Jr., and E. C. Crume, Jr. Plasma transport coefficients for nonsymmetric toroidal confinement systems. *Phys. Fluids*, 29(9):2951–2959, 1986.

[4] C. D. Beidler and W. D. D'haeseleer. A general solution of the ripple-averaged kinetic equation. *Plasma. Phys. Contr. Fusion*, 37:463–490, 1995.

[5] C. D. Beidler, K. Allmaier, M. Yu. Isaev, S. V. Kasilov, W. Kernbichler, G. O. Leitold, H. Maaßberg, D. R. Mikkelsen, S. Murakami, M. Schmidt, D. A. Spong, V. Tribaldos, and A. Wakasa. Benchmarking of the mono-energetic transport coefficients - results from the international collaboration on neoclassical transport in stellarators (icnts). *Nucl. Fusion*, 51(7):076001, 2011.

[6] V. Tribaldos. Monte Carlo estimation of neoclassical transport for the tj-ii stellarator. *Phys. Plasmas*, 8:1229–1239, 2001.

[7] M. Yu. Isaev, S. Brunner, W.A. Cooper, T.M. Tran, A. Bergmann, C.D. Beidler, J. Geiger, H. Maassberg, J. Nhrenberg, and M. Schmidt. Venus+δf: A bootstrap current calculation module for 3-d configurations. *Fusion Sci. Technol.*, 50:440–446, 2006.

[8] K. Allmaier, S. V. Kasilov, W. Kernbichler, and G. O. Leitold. Variance reduction in computations of neoclassical transport in stellarators using a δf method. *Phys. Plasmas*, 15:072512, 2008.

[9] W. Kernbichler, S. V. Kasilov, G. O. Leitold, V. V. Nemov, and K. Allmaier. Recent progress in NEO-2 - A code for neoclassical transport computations based on field line tracing. *Plasma and Fusion Research*, 3:S1061–1–S1061–4, 2008.

[10] M. Landreman, H. M. Smith, A. Mollén, and P. Helander. Comparison of particle trajectories and collision operators for collisional transport in nonaxisymmetric plasmas. *Phys. Plasmas*, 21(4):042503, 2014.

[11] V. V. Nemov, S. V. Kasilov, W. Kernbichler, and M. F. Heyn. Evaluation of $1/\nu$ neoclassical transport in stellarators. *Phys. Plasmas*, 6(12):4622–4632, 1999.

[12] W. Kernbichler, S. V. Kasilov, G.O. Leitold, V.V. Nemov, and N.B. Marushchenko. Generalized spitzer function with finite collisionality in toroidal plasmas. *Contrib. to Plasma Physics*, 50(8):761–765, 2010.

[13] W. Kernbichler, G. Kapper, S. V. Kasilov, and N.B. Marushchenko. Computation of the spitzer function in stellarators and tokamaks with finite collisionality. *EPJ Web of Conferences*, 87:01006, 2015.

[14] S. V. Kasilov, W. Kernbichler, A. F. Martitsch, H. Maassberg, and M. F. Heyn. Evaluation of the toroidal torque driven by external non-resonant non-axisymmetric magnetic field perturbations in a tokamak. *Phys. Plasmas*, 21(9):092506, 2014.

[15] V. V. Nemov. Calculations of the magnetic surface function gradient and associated quantities in a torsatr. *Nucl. Fusion*, 28:1727–1736, 1988.

[16] K. C. Shaing and J. D. Callen. Neoclassical flows and transport in nonaxisymmetric toroidal plasmas. *Phys. Fluids*, 28(11):3315–3326, 1983.

[17] N. Nakajima, M. Okamoto, J. Todoroki, Y. Nakamura, and M. Wakatani. Optimization of the bootstrap current in a large helical system with $l = 2$. *Nuclear Fusion*, 29(4):605–616, 1989.

[18] A. H. Boozer and H. J. Gardner. The bootstrap current in stellarators. *Phys. Fluids B*, 2:2408–2421, 1990.

[19] S. V. Kasilov and W. Kernbichler. Passive cyclotron current drive efficiency for relativistic toroidal plasmas. *Phys. Plasmas*, 3(11):4115–4127, 1996.

[20] P. Helander and P. J. Catto. Neoclassical current drive by waves with a symmetric spectrum. *Phys. Plasmas*, 8(5 II):1988–1994, 2001.

[21] K. C. Shaing, S. A. Sabbagh, and M. S. Chu. An approximate analytic expression for neoclassical toroidal plasma viscosity in tokamaks. *Nuclear Fusion*, 50(2):025022, 2010.

[22] C. G. Albert, M. F. Heyn, S. V. Kasilov, W. Kernbichler, and A. F. Martitsch. Toroidal rotation in resonant regimes of tokamak plasmas due to non-axisymmetric perturbations in the action-angle formalism. In *42nd EPS Conference on Plasma Physics*, volume 39E, page P1.183, Lisbon, Portugal, 2015. European Physical Society.

[23] A. H. Boozer. Enhanced transport in tokamaks due to toroidal ripple. *Phys. Fluids*, 23(11):2283–2290, 1980.

[24] V. S. Tsypin, A. B. Mikhailovskii, R. M. O. Galvao, I. C. Nascimento, M. Tendler, C. A. de Azevedo, and A. S. de Assis. Plasma rotation in toroidal devices with circular cross-sections. *Phys. Plasmas*, 5(9):3358–3365, 1998.

[25] K. C. Shaing, M. S. Chu, and S. A. Sabbagh. Eulerian approach to bounce-transit and drift resonance and neoclassical toroidal plasma viscosity in tokamaks. *Plasma. Phys. Contr. Fusion*, 51(5):075015, 2009.